ELSEVIER

Contents lists available at ScienceDirect

Chemical Engineering Science

journal homepage: www.elsevier.com/locate/ces



Supervised machine learning for prediction of zirconocene-catalyzed α -olefin polymerization



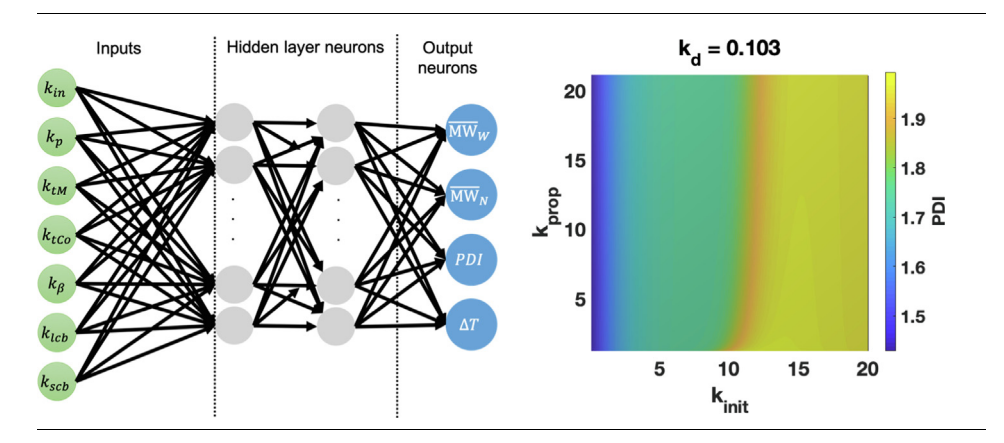
Benjamin A. Rizkin, Ryan L. Hartman*

New York University, Department of Chemical and Biomolecular Engineering, 6 MetroTech Center, Brooklyn, NY 11201, United States

HIGHLIGHTS

- Neural networks can be used to analyze metallocene catalysis reactions
- Successfully predicted molecular weight, polydispersity and reactor temperature.
- Experimental space visualized and connections between parameters made
- Network used to predict rate constants from observable data.

G R A P H I C A L A B S T R A C T



ARTICLE INFO

Article history: Received 13 June 2019 Received in revised form 14 August 2019 Accepted 14 September 2019 Available online 14 September 2019

Keywords: Polymerization Process development Machine learning Neural networks Metallocene catalysis Olefins

ABSTRACT

A new approach is demonstrated in which an Artificial Neural Network (ANN) was trained with first-principles data to predict the chain length, polydispersity (Đ) and adiabatic temperature for a zirconocene-catalyzed polymerization reaction. The ANN-generated data shows good agreement with the theoretical results, with an overall R² of 0.9987. Using its significantly enhanced computational speed, the ANN was used to analyze the reaction space, providing insights into trends seen in molecular weight and Đ with various combinations of kinetic parameters, particularly pointing out regions of desirable and undesirable operation. The network was trained in reverse and used to generate reaction rate constants from chain length and Đ, enabling a new form of kinetic deduction for polymerization reactions. This training was used to derive potential rate constants for different catalysts reported in the literature. Overall, this data indicates that ANNs are a plausible tool for analyzing data from complex metallocene-catalyzed olefin polymerizations.

© 2019 Elsevier Ltd. All rights reserved.

E-mail address: ryan.hartman@nyu.edu (R.L. Hartman).

Abbreviations: ANN, Artificial Neural Network; a/act, activation; β, -hydride elimination; Cat, catalyst; Cocat, cocatalyst; d, deactivation; DFT, Density Functional Theory; D (i), dead polymer chain with *i* monomers; D=(i), dead polymer chain detached from catalyst; i/init, initiation; K_a , rate of catalyst activation; k_{init} , rate of chain initiation; k_p , rate of chain propagation; k_a , rate of spontaneous deactivation; k_{tt} , rate of chain transfer to hydrogen; k_{tt} , rate of chain transfer to monomer; k_{tCo} , rate of chain branching; lcb, long chain branching; ML, Machine Learning; M, monomer; M_N , Mn, Number Average Molecular Weight; M_W , Mw, Weight Average Molecular Weight; PDI, D, Polydispersity Index; P(0), active catalyst; P(i), polymer chain on catalyst site with *i* monomers; $P_d(0)$, deactivated catalyst; P'(i), branched polymer chain; p/prop, propagation; QSAR, Quantitative Atructure—Activity Relationship; RMSE, Root Mean Square Error; scb, short chain branching; tM, chain transfer to monomer; tH, transfer to hydrogen; tM, transfer to monomer; tCo, transfer to cocatalyst (activator).

^{*} Corresponding author.

1. Introduction

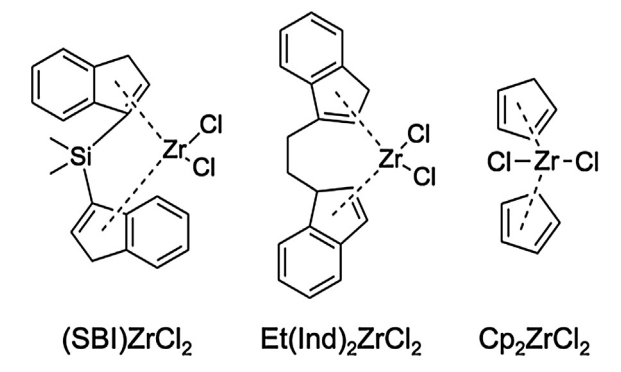
1.1. Machine learning

Machine Learning (ML) is a form of predictive analytics which uses a training dataset to develop a mathematical model for extrapolating conclusions from input data. Artificial Neural Networks (ANNs) are one example of ML and are a powerful tool for modeling complex systems and processes with multiple inputs and nonlinear behavior. In essence a neural network works in much the same way as a brain, by summing the values of inputs, normalizing them, and triggering a feedforward cascade to other neurons. The field of applying ANNs to studies of catalytic performance originated in 1994 with the papers of Kite et al. who used neural networks to examine the oxidative dehydrogenation of ethylbenzene (Kite et al., 1994) and Sasaki et al. who used the technology to investigate NO decomposition over a Cu/ZSM-5 zeolite catalyst (Sasaki et al., 1995). Molga et al. used ANNs to model the complex reaction system kinetics of the oxidation of 2octanol, successfully predicting the concentration and heat flow profiles in a semi-batch reactor, but were not successful in generalizing their results between runs (Molga et al., 2000). Saber et al. used ANNs to estimate reaction rates for methanol dehydration which they successfully used to replace complex analytical equations (Valeh-E-Sheyda et al., 2010). Finally, Hough et al. used machine learning as a tool for process optimization in biomass pyrolysis and Nandi et al. used an ANN in conjunction with a genetic algorithm for the optimization of zeolites for benzene hydroxylation (Hough et al., 2017; Nandi et al., 2002). Since then there have been many contributions to the field including works related to heterogeneous catalysis, biological catalysis, materials science, petrochemical engineering, green chemistry and even first-principles research.^{3–18} Most of these examples, along with the work presented here, use supervised machine learning where there is a set of known values to train the system. For other problems unsupervised learning may be used, particularly in situations where the right output is not known. Overall, ML has become a powerful tool for research due to its ability to analyze complex trends in highly multivariate data.

The prevalence of using machine learning as a research tool in these areas has been gaining popularity because it brings a level of abstraction to the approximation of highly multidimensional problems. However, there is also a disadvantage due to a lack of insight into the physical basis of the solution, only an abstract model (akin to a general solution to a PDE versus the PDE itself). Additionally, for the machine learning approach to be successful at representing the physics of the problem a large and statistically robust data set must be used. In recent years Artificial Intelligence (AI) has found favor in chemical engineering for modeling of complex processes not easily amenable to numerical analysis, such as the prediction of operating characteristics of industrial equipment. Work has been done to use AI in modeling of unit operations and chemical processes including studies about distillation (Diwekar and Madhavan, 1991), polymerizations (Chan and Nascimento, 1994; Curteanu et al., 2014; Curteanu and Leon, 2008; Leite et al., 2007; Nayak and Gupta, 2004), depolymerizations (Fazilat et al., 2012), materials design (Giro et al., 2005; Polikar et al., 2001; Zhang and Friedrich, 2003), reaction modeling (Hough et al., 2017; Irfan et al., 2012; Kite et al., 1994; Molga et al., 2000; Nakazaki and Inui, 1989; Nandi et al., 2002; Papes Filho and Maciel Filho, 2010; Sasaki et al., 1995; Valeh-E-Sheyda et al., 2010) and several review papers (Goncalves et al., 2013; Himmelblau, 2000; Mohd Ali et al., 2015; Ruiz et al., 2000; Sadiku et al., 2017; Schwaller et al., 2018). Finally there have been relevant recent developments by Ahmadi et al. (2009) who used ANNs to model the polymerization rate of ethylene and Charoenpanich et al. (2016) who used neural networks to model microstructures of ethylene/1-olefin copolymers. In this work one potential application of this new modeling approach is shown in the prediction of polymer characteristics from a multi-step metallocene alpha(olefin) polymerization reaction. The training set is derived from a series of first-principles differential species balances. The performance of the resulting ML solution is then compared with literary data to check the validity of the solution.

1.2. Metalocene catalysis

There have been many recent studies of zirconocene catalysts, including both computational and experimental work. Since the original works by Kaminsky (Kaminsky et al., 1985; Kaminsky and Spiehl, 1989), Woo (Woo and Tilley, 1989), Brintzinger (Kaminsky et al., 1985; Krauledat and Brintzinger, 1990; Lenton et al., 2013) and Herrmann (Herrmann et al., 1989) multiple groups have been tackling this complicated problem. An overview of a few representative structure types can be seen in Scheme 1. These works were followed by investigations of the structure by Bochmann et al. (1994) and continued by Christopher et al. (1996). Kawamura-Kuribayashi et al. have worked extensively to develop Molecular Orbital (MO) and Molecular Mechanics (MM) models of these catalytic processes (Kawamura-Kuribayashi et al., 1992). Song et al. have worked to determine the role of the anion in the polymerization process (Song et al., 2004b), along with Soga and Kaminaka (1993) who investigated the effects of different activators. Other kinetic studies were conducted by Song et al. (2003) using a quenched-flow kinetic experiment and by Moscato et al. (2012) using a chromophore labeled catalyst with in-situ NMR and UV-Vis characterization. Additionally, Quantitative Structure-Activity Relationship (QSAR) computational studies has been carried out, yielding insight into the intricacies of the active site and the catalytic mechanism (Cruz et al., 2004, 2014, 2007a, 2007b, 2005; Drummond and Sumpter, 2007; Martínez et al., 2012; Möhring and Coville, 2006; Yu et al., 2019), along with a DFT study was by Hölscher et al. (2002). Yu et al. used a novel labeling method utilizing methyl propargyl ether (MPE) as a labeling agent to better understand the active sites in a Ziegler-Natta polymerization (Yu et al., 2019). Additional kinetic experiments were carried out by (Chan and Nascimento, 1994; Chen and Marks, 2000; Christopher et al., 1996; Ibrehem et al., 2008; Inkson et al., 2006; Kaminsky and Steiger, 1988; Kim and Nam Hwang, 1998; Resconi, 1999; Rieger and Janiak, 1994; Song et al., 2003; Wang et al., 2005; Yasin et al., 2005), just to name a few.



Scheme 1. Three different types of zirconocene single-site polymerization catalysts, from left to right are (SBI)ZrCl₂ (Song et al., 2003), Et(Ind)₂ZrCl₂ (D'Agnillo et al., 1998) and Cp₂ZrCl₂ (Song et al., 2003).

Overall alpha(olefin) polymerization catalysis is a major topic of research to this day, mainly due to its relevance to the largest quantity commodity plastics in the world.

Overall metallocene alpha-olefin polymerization catalysts exhibit characteristics which make them desirable for a range of applications. First, these catalysts are active at ambient conditions, removing the need for extreme conditions in the reactor. Traditional poly(ethylene) and poly(propylene) processes rely upon high temperature and pressure reactors, which not only use exponentially more energy, but also present safety concerns. Second, these catalysts allow for the very precise tailoring of polymer properties, allowing for optimized materials. By tuning the properties of the catalyst molecule such as the stereochemistry, it becomes possible to make polymers with different tacticities and structures (Kaminsky, 1994). Additionally, by modifying the activator composition, reaction concentrations and conditions, it becomes possible to tune the chain length, degree of branching and polydispersity of the resultant polymer (Dare et al., 2004; Rieger and Janiak, 1994). However, due to the complex synthesis pathways and fragile chemistry, these catalysts have only gained adoption in select parts of the olefin polymerization market (Hutley and Ouederni, 2016). Overall the broad range of metallocene single-site catalysts provides interesting advantages for the tuning of polymer properties for ideal industrial applicability but require precise optimization to be economical.

In general, metallocenes for polymerization of propylene, ethylene, 1-hexene and other alpha-olefins exhibit several stages in the catalytic cycle. The first step is initiation where a metal-alkyl bond is formed. Next is propagation where monomer units are inserted into the growing polymer chain, which could happen in a 1,2- or 2,1- direction. The final step is deactivation or termination. There are also many possible intermediate and final steps including chain transfer, beta-hydride elimination and chain transfer to various species, which depend on the specific catalyst/activator/monomer combination being investigated (Prakash, 2013). For kinetic determination and quantification of new catalysts three of these steps are largely important: initiation (k_{init}) , propagation (k_{prop}) and spontaneous catalyst deactivation (k_d) , which are for the most part universal between catalyst systems. The resultant polymer is either isotactic, atactic, or a mixture thereof depending on the chiral mixture of the catalyst (Ewen, 1984). Relevant mechanistic studies include the work of Guo et al. who investigated homopolymerizations and co-polymerizations with ethylene and propylene (Guo et al., 2017), Pletcher et al. who compared Group IV Bis-Phenolate catalysts (Pletcher et al., 2016), Henson et al. who looked at slurry polymerization using a racemic catalyst (Gonzalez-Ruiz et al., 2006), Klothammer et al. who used Attenuated Total Reflectance Fourier Transform Infrared Spectroscopy (ATR-FT-IR) to obtain kinetic information (Kolthammer et al., 1992) along with the work of Lin et al. and Subramanyam et al. who did a fundamental kinetic study (Lin et al., 2000; Subramanyam and Sivaram, 2007) and Christianson et al. who used stop-flow NMR (Christianson et al., 2010). However, despite all of these studies there still remains a gap in the link between reaction rate constants and polymer characteristics, along with inconsistent reports of kinetic parameters between publications, with a summary of several example publications seen in Table 1. Understanding the reaction mechanism and reaction domain topology of alkene polymerization reactions has been of significant interest, especially to industry.

Our overall goal is to investigate machine learning as an efficient and robust tool for approximating the behavior of zirconocene-catalyzed alpha-olefin polymerizations and to use this information to gain insight into the broad reaction space in which these polymerizations take place. The work further establishes a link between physically observable characteristics and reaction rate constants, allowing for ex situ analysis and interpretation of kinetic information. The ANN approach offers two benefits over first-principles calculations, the first being the ability to create solutions much quicker and with more limited computational power, and the second being the possibility of solving the system in reverse, which is not possible with the traditional differential mass balance approach. This has possible applications in industrial control and operation of catalytic polyolefin production processes in which marginal shifts in reaction characteristics can have a strong influence on commercially relevant properties. It also has potential application in research by removing the necessity to monitor labeled active sites or other markers in order to establish a link between the produced polymer and the catalytic cycle.

2. Methods

2.1. Reaction mechanism

Generation of the dataset began with a series of reaction steps and the resulting differential mass balances along the methodology of (Ahmadi et al., 2009; Prakash, 2013; Song et al., 2003; Young and

Table 1Comparison of kinetic and polymer characteristic information for the polymerization of 1-hexene provided from the literature. Check marks represent data which is available in the publication, crosses represent data which is not reported and "-" represents data interpolated using the correlation $\mathfrak{D} = MW_w/MW_n$.

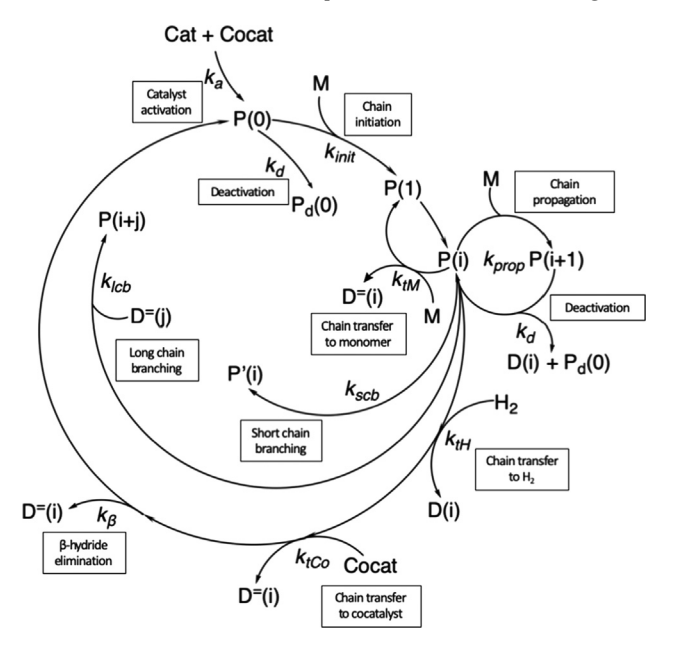
Publication	Catalyst	Activator	Monomer	Kinetic information reported	MW_{w}	MW_n	Đ
(Ghiotto et al., 2013)	rac-Me ₂ Si(2-Me-Benz[e]Ind) ₂ ZrCl ₂	MAO	1-hexene	$\begin{aligned} k_{init} \sim 3.8 \\ k_{prop} \sim 1.0 \\ k_d \sim 27 \end{aligned}$	~	/	~
(Moscato et al., 2012)	(SBI)ZrCH ₂ SiMe ₂ (C ₆ H ₄)NMe ₂	$MeB(C_6F_5)_3$	1-hexene	$\begin{aligned} k_{init} \sim 0.004 \\ k_{prop} \sim 1.0 \\ k_d \ \times \end{aligned}$	×	×	×
(Moscato et al., 2010)	rac-(SBI)Zr(Chrom)Me	$MeB(C_6F_5)_3$	1-hexene	$\begin{aligned} k_{init} &\sim 0.0001 \\ k_{prop} &\sim 0.4 \\ k_d &\times \end{aligned}$		_	~
(Song et al., 2004a)	(SBI)Zr(CH ₂ SiMe) ₃	$B(C_6F_5)_4$	1-hexene	$egin{array}{l} k_{init} imes \\ k_{prop} & highly & varried \\ k_d imes \\ \end{array}$	×	×	×
(Zhao et al., 2000)	$rac-(dimethyl silyl) bis (4,5,6,7-tetra hydro-1-indenyl) ZrCl_4 \\$	MAO	1-hexene	$\begin{array}{l} k_{init} \times \\ k_{prop} \times \\ k_{d} \times \end{array}$	_	✓	~
(Liu et al., 2001)	rac-(C2H4(1-indenyl) ₂)ZrMe	$MeB(C_6F_5)_3$	1-hexene	$\begin{array}{l} k_{init} \times \\ k_{prop} \times \\ k_{d} \times \end{array}$	×	×	×
(Switzer et al., 2012)	Zr(tBu-ONNMe ₂ O)	$B(C_6F_5)_3$	1-hexene	$\begin{array}{l} k_{init} \sim 0.1 \\ k_{prop} \sim 11 \\ k_{d} \times \end{array}$	×	×	×

Ma, 2002), with the exact series of balances being those derived by Prakash (2013) with a plausible lower range of reaction rate constants being taken from Moscato et al. (2012), who studied the reaction under NMR using conditions tailored for a lower reaction rate. The series of reaction steps can be seen below and in Scheme 2.

- 1. $Cat + Cocat \xrightarrow{k_a} P(0)$
- 2. $P(0) + M \stackrel{k_{init}}{\rightarrow} P(1)$
- 3. $P(i) + M \xrightarrow{k_p} P(i+1)$
- 4. $P(i) \xrightarrow{k_d} P_d(0) + D(i)$
- 5. $P(0) \xrightarrow{k_d} P_d(0)$
- 6. $P(i) + H_2 \stackrel{k_{tH}}{\to} D(i) + P(0)$
- 7. $P(i) + M \xrightarrow{k_{tM}} D^{-}(i) + P(1)$
- 8. $P(i) + Cocat \stackrel{k_{tCo}}{\to} D^{-}(i) + P(0)$
- 9. $P(i) \xrightarrow{k_{\beta}} D^{=}(i) + P(0)$
- 10. $P(i) + D^{=}(j) \stackrel{k_{lcb}}{\to} P(i+j)$
- 11. $P(i) \stackrel{k_{scb}}{\rightarrow} P'(i)$

2.2. Network training

To perform the ANN training, a dataset of 2000 possible combinations of reaction rate constants was formulated by combining constants from literature with random small up and down changes as an input to the differential species balances. The small changes were made as perturbations to the average literary values in order to adequately sample the entire space of possible reaction rate constants. The combination of rate constants was used in order to fully encompass the range of possible values. This moderately sized dataset was then used to train a neural network with 70% of the data being used for training, 15% for validation and 15% for testing. Since the initial conditions for the generation of the training set were already randomized, and the form of the distribution was known, retaining a 70/15/15 split was sufficient and it was not necessary to further randomize the samples or perform bootstrapping (Paass, 1993). The full dataset was used in the generation of all figures that follow. Based on a comparison of different training meth-



Scheme 2. Generalized catalytic cycle for the polymerization of ethylene using a metallocene catalyst.

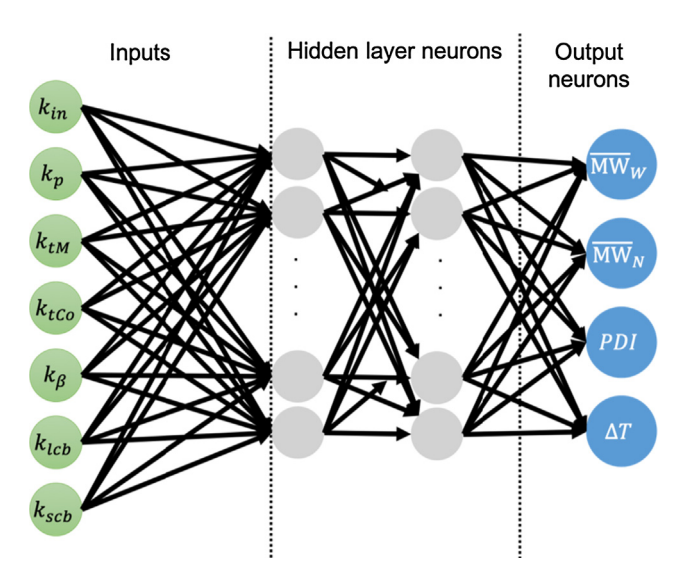


Fig. 1. Model of the neural network used for the prediction of polymer characteristics based on kinetic information about the catalyst. The network used two hidden layers each with 15 neurons and a Levenberg-Marquardt training algorithm, as this combination gave the highest fit fidelity (see Fig. 3). The network was used to predict the number and weight average molecular weights (MW_n, MW_w), polydispersity index (PDI) and adiabatic temperature change (ΔT).

ods and numbers of hidden layer neurons a Levenberg-Marquardt training algorithm was used with 15 hidden neurons per layer and two layers. A full breakdown of the training results can be seen in Fig. 3. A diagram of the network can be seen in Fig. 1 and the dataflow for the experiment can be seen in Fig. 2. All hidden layer weights and biases were computed automatically using the neural network training function in MATLAB. Overall, the training dataset was formulated using the 11-step reaction mechanism and then used to train the ANN, which in turn was checked using additional calculations and used to make predictions.

Analysis of these differential equations and training of the ANNs was performed by using MATLAB R2018b and the ODE45 toolkit running on dual Intel Xeon E5620 quad-core CPUs with 20 GB of DDR3 memory.

3. Theory

3.1. Differential balances

The reaction steps enumerated above were used to construct a series of differential mass balances as can be seen below. Again, this analysis used the work of Prakash (2013) in an effort to use validated literary assumptions and methods.

- 1. $r_{cat} = -k_a[Cat][Cocat]$ 2. $r_{P(0)} = k_a[Cat][Cocat] - k_{init}[M][P(0)] - k_d[P(0)] +$ $k_{tH}[H_2]\lambda_0^l + k_{tCo}[Cocat]\lambda_0^l + k_{\beta}\lambda_0^l$ 3. $r_{P_{d(0)}} = k_d ([P(0)] + \lambda_0^l)$ 4. $r_{Cocat} = -k_a[Cat][Cocat] - k_{tCo}[Cocat]\lambda_0^l$
- 5. $r_M = -k_{init}[M][P(0)] k_p[M]\lambda_0^l k_{tM}[M]\lambda_0^l$
- 6. $r_{H_2} = -k_{tH}[H_2]\lambda_0^l$
- 7. $r_{P(i)} = -k_{prop}[M][P(i)] + k_{prop}[M][P(i-1)] k_d[P(i)] + k_{tH}[H_2][P(i)] k_{tM}[M][P(i)] k_{tCo}[Cocat][P(i)] k_{\beta}[P(i)] k_{lcb}[P(i)]\lambda_0^- k_{scb}[P(i)]$
- 8. $r_{D(i)} = k_d[P(i)] + k_{tH}[H_2][P(i)]$
- 9. $r_{D^{=}(i)} = k_{tM}[M][P(i)] + k_{\beta}[P(i)] + k_{tCo}[Cocat][P(i)] k_{lcb}[P(i)]\lambda_{0}^{=}$
- 10. $r_{P(i+j)} = k_{lcb}[P(i)]\lambda_0^{=}$
- 11. $r_{P'(i)} = k_{scb}[P(i)]$

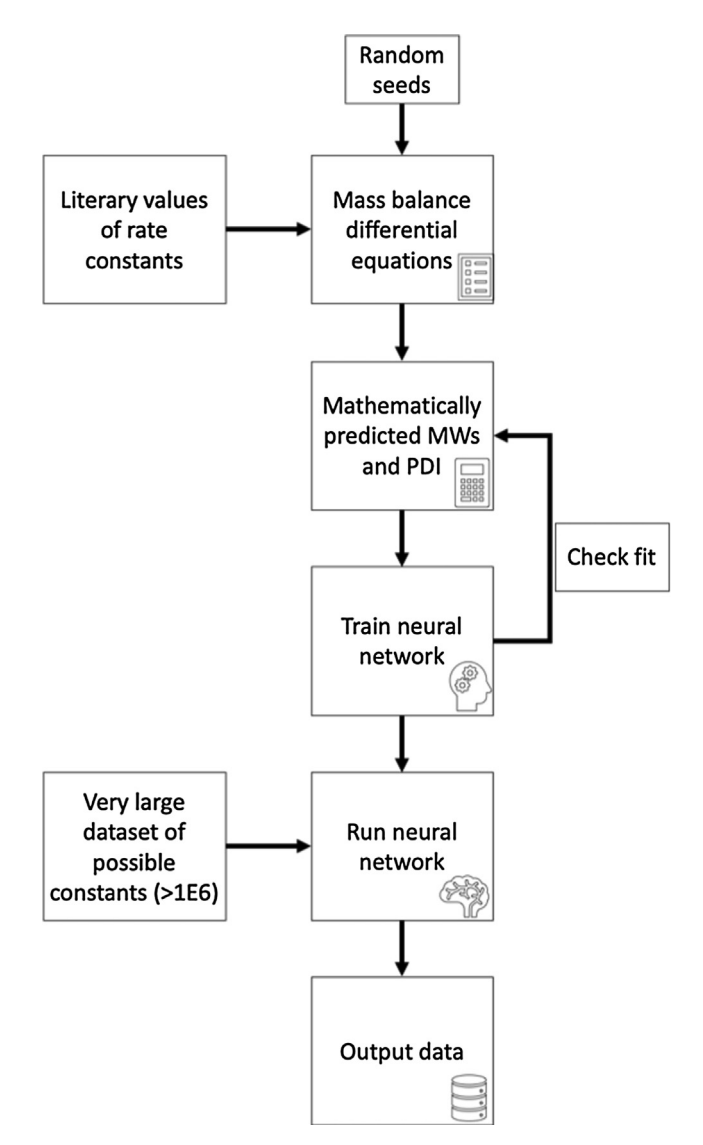


Fig. 2. Data flow for the computational experiment. A training dataset is first generated using a literary model with an augmented input matrix consisting of validated rate constants with randomly fluctuating seeds to augment the range of values. This dataset is used to train the neural network which is then in turn used to make predictions.

3.2. Method of moments and parameter estimation

These balance equations are then used to derive the moments of chain length distribution (CLD) for living $(\lambda_0^l, \lambda_1^l, \lambda_2^l)$, dead $(\lambda_0, \lambda_1, \lambda_2)$, and dead with terminal double bond $(\lambda_0^=, \lambda_1^=, \lambda_2^=)$ polymer chains. Living polymer chains are ones which are still actively polymerizing, dead chains are no longer polymerizing and dead with terminal double bond chains have a double bond at or proximal to the end of the chain (Hildenbrand et al., 1982).

Next, the number average and weight average molecular weights are computed from the moments of chain length distributions.

1.
$$\overline{M}_n = 28.05 * (\lambda_1^l + \lambda_1 + \lambda_1^-)/(\lambda_0^l + \lambda_0 + \lambda_0^-)$$

2.
$$\bar{M_W} = 28.05 * (\lambda_2^l + \lambda_2 + \lambda_2^=)/(\lambda_1^l + \lambda_1 + \lambda_1^=)$$

$$\mathbf{3.} \ \ \bar{\mathrm{PDI}} = \left(\left(\lambda_2^l + \lambda_2 + \lambda_2^= \right) \left(\lambda_0^l + \lambda_0 + \lambda_0^= \right) \right) / (\lambda_1^l + \lambda_1 + \lambda_1^=)$$

This same methodology can be used to get other parameters of interest such as polymerization rate and the number of long and short chain branches in an average polymer chain.

Finally the adiabatic temperature change can be calculated as $T = ([-\Delta H_{Rx}(T_0)]X)/(\sum_{i=1}^n \Theta_i C_{P_i})$, where T is the temperature, $-\Delta H_{Rx}$ is the exotherm of reaction, T_0 is the initial temperature, X is the conversion and $\sum_{i=1}^n \Theta_i C_{P_i}$ is the weighted average heat capacity of the solution.

This analysis assumes a homogeneous, well-mixed, adiabatic batch reactor, which allows for the separation of kinetic and transport phenomena in the analysis, removing dependence on a specific reactor system. In industry numerous different types of reactor systems are used, ranging from high pressure gas-phase to moderate condition liquid-phase with various arrangements of sidestream feeds and mixing devices (Galli et al., 2011; Kaminsky, 2011). In academic studies an even broader range of devices is used, including microfluidic or very high pressure systems (Kaminsky, 2011). Adaptation of this methodology to a particular reactor system would involve an extra series of differential equations accounting for heat and mass transfer for the chosen system. which will vary greatly between applications. Mass transfer may affect the outcome of polymerization reactions as the viscosity of the solution increases. Increasing viscosity would lead to decrease of monomer at catalyst active sites and thus decrease the overall yield of polymer. However, this is highly dependent on the application as types of catalyst, reactors, feed streams and gelling characteristics all vary widely (MacGregor, 1986).

4. Results and discussion

4.1. Network fit characterization

Upon generating the training dataset and a validation set the network was trained and the quality of the fit was analyzed. Neural network predictions were made for the Weight Average Molecular Weight (MW_N, Mw), Number Average Molecular Weight (MW_N, Mn), Polydispersity Index (PDI, Φ) and the adiabatic temperature change. The rate of activation was assumed very fast and constant between all the trials, consistent with the work of Prakash (2013). Statistical analysis was performed on this data to verify the suitability of the ANN modeling approach to polymerization data. For the polymer characteristics prediction network, it was observed that the experimental (ANN-predicted) values closely matched the theoretically predicted (species balance-based) targets. A fit regression plot for the network can be seen in Fig. 3 below, along with a comparison of different network architectures.

It is observed that for ΔT , D and MW the ANN predictions lies in overall good agreement with the first-principles differential special balance model. Next, basic statistical tests analysis was conducted on all the output parameters. In Table 2 it can be seen that overall the network represents the data with an R^2 -value of 0.9987 between all the output data points. A P-test indicates a value of zero, meaning that the null hypothesis is statistically false. Finally, a Kolmogorov-Smirnov (KS) test is carried out on the data, returning a value of 1, indicating that the data does not in a whole represent a normal distribution. In Table 3 it is observed that the Root Mean Square Error (RMSE) between the predicted and target values lies within a relatively tight error band, indicating plausible predictions. Overall these statistical tests indicate that the predicted data matches the targets in a statistically reasonable manner.

4.2. Reaction space topology visualization and analysis

The next step in the investigation was to use the ANN to generate a very large sample range of possible kinetic parameters and to test the effects these would have on the measured parameters. A set of values was generated for k_{init} , k_{prop} and k_d and the neural

network was run over this range, holding the other parameters constant. A study of the different permutations leads to the data in Figs. 4–6. Analysis of these figures allows for interpretation of the experimental space and for a quick visual way to assess the impacts of different combinations of parameters.

In Fig. 4 the effect of the various kinetic constants on $\overline{\text{MW}}$ can be seen, with the top plot indicated a low k_d , then the middle a medium k_d and the bottom a high k_d , all over the same range of k_{init} and k_{prop} . These results suggest that lower values of k_{init} result in a lower average molecular weight, with k_d having a strong inverse correlation to molecular weight. This can be explained logically because as the frequency of initiating polymer chains increases statistically it is more probable for chains to have a larger distribution of lengths. Also, as the death rate of chains increases it is more probable that chains are terminated at a shorter length. Additionally it is observed that the ratio of k_{prop} to k_d has a strong influence on the number average molecular weight, with an increasing ratio

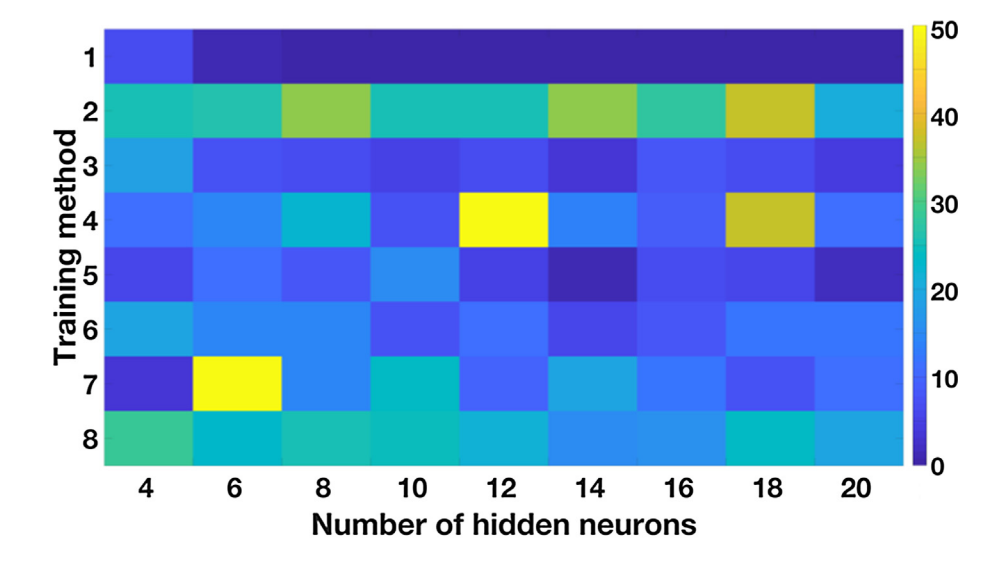
 Table 2

 Statistical test characteristics for overall ANN fit quality.

Statistical test	Value
R ² -value	0.9987
P-test	0
KS-test	1

Table 3 RMSE fit characteristics for ANN output.

Data point	RMSE	RMSE (percent)
$\stackrel{-}{MW_W}$	0.8518	0.2599
\widetilde{MW}_n	1.6977	0.2705
Đ	0.1118	5.8411
Adiabatic ΔT	7.9865	0.3535



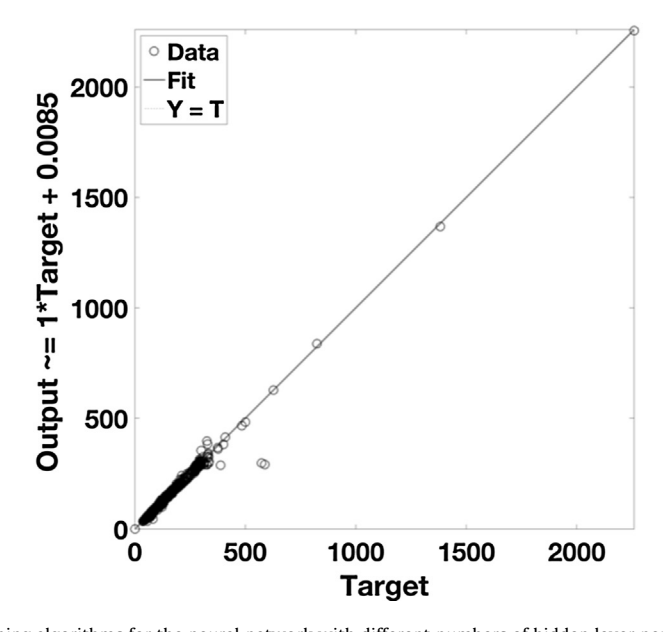


Fig. 3. (Top) Comparison of different training algorithms for the neural network with different numbers of hidden layer neurons, with the fit indicated as the Mean Square Error (lower is better). Algorithms: 1 = Levenberg-Marquardt (Damped Least Squares), 2 = quasi-Newton backpropagation, 3 = Resilient backpropagation (RProp), 4 = Scaled conjugate gradient backpropagation backpropagation with Pletcher-Reeves updates, 6 = Conjugate gradient backpropagation with Powell-Beale restarts, 7 = Conjugate gradient backpropagation with Polak-Ribiére updates, 8 = One-step secant backpropagation. (Bottom) Regression plot displaying the network inputs versus targets. This plot shows the predictive quality of the neural network as derived from the training function in MATLAB, using an equally-weighted combination of the all the fitted factors, thus showing overall network fit quality. Fit quality (R-value) for validation and test datasets was 0.9987.

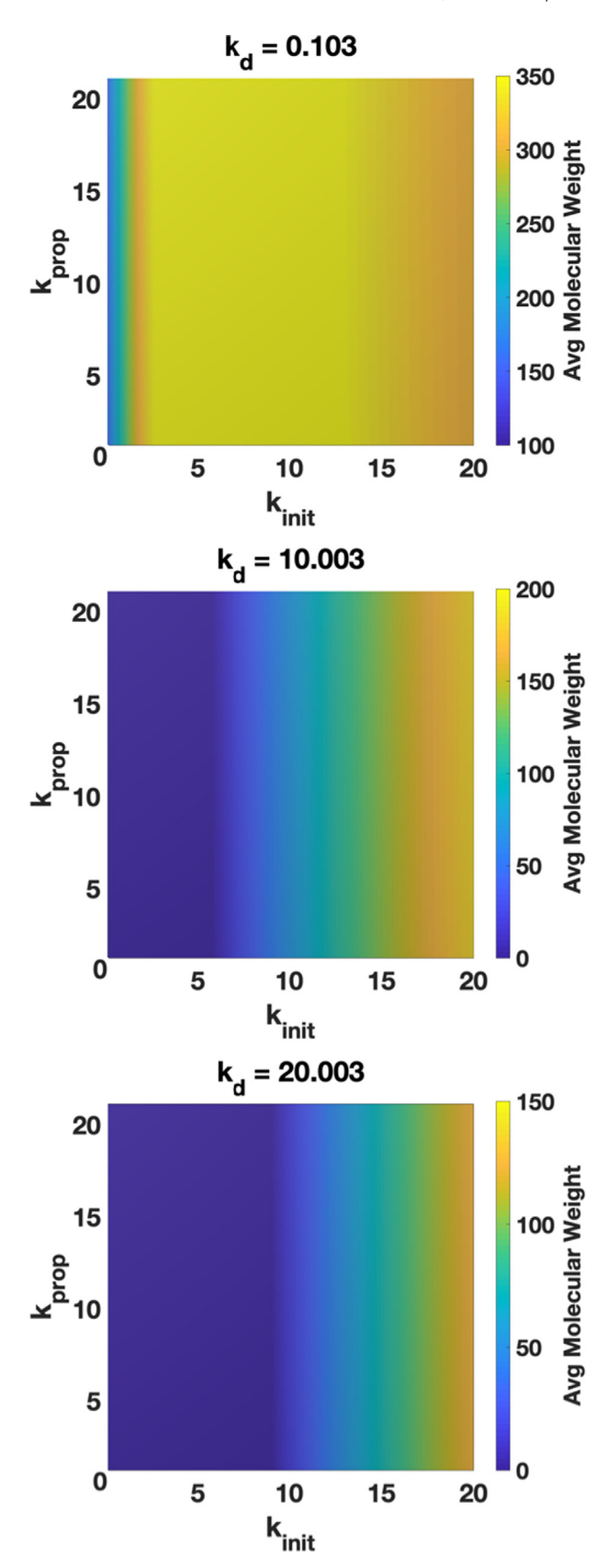


Fig. 4. Heatmaps for \overline{MW}_n (×10²) over a range of k_{init} , k_{prop} and k_d .

leading to larger chains, with the results being summarized in Fig. 5.

Next, a similar analysis is carried out on the Đ, with the results being summarized in Fig. 6. It is observed that as the rate of initi-

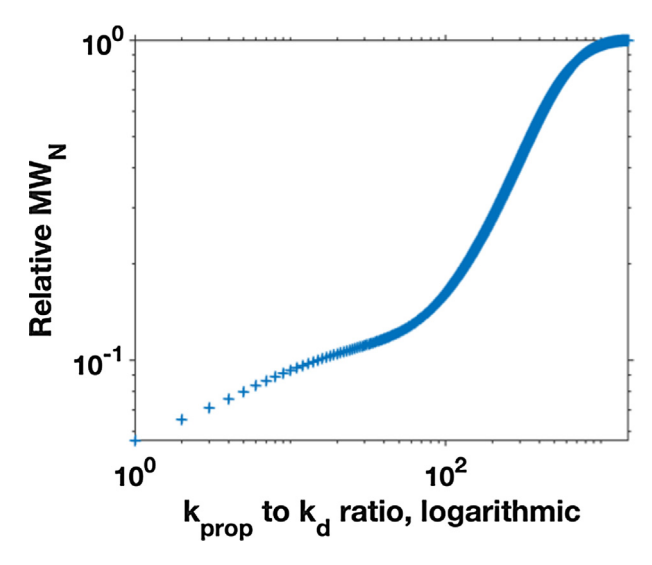


Fig. 5. Correlation between the relative number average molecular weight (MW divided by maximum MW) to the ratio of the rate constants of propagation and chain death. A positive correlation is observed, indicating that relatively higher values of k_{prop} result in larger chain lengths.

ation increases the Đ also increases, with an inverse correlation being seen for the death rate of chains. It is also observed that the rate of propagation has little effect on the Đ, which is mainly a function of the initiation rate. A similar theoretical explanation can be offered as for the average chain length, as the number of initiated chains increases so does the distribution of chain lengths, while as the death rate of the chains increases the Đ becomes lower because chains are terminated faster.

Finally, the effect of the different parameters is observed on the final adiabatic temperature of the reactor, and the summary of these results can be seen in Fig. 7. The maximum temperature changes are seen at high rates of propagation, which can be explained because as the chain is growing more π bonds are being converted to σ bonds, releasing large amounts of energy. As the initiation rate increases, the final temperature also appears to increase, as more new chains are being nucleated. Finally, as the death rate increases the temperature drops off quickly, as relatively more active catalyst is being removed from the system and more of the monomer remains unreacted.

4.3. Reverse prediction training and fit characterization

The next step of the investigation involved training the network in reverse, meaning it would predict a possible combination of kinetic parameters given the molecular weight and Đ of a sample. The utility of this approach is that kinetic information can be deduced from parameters which can be measured ex situ, This would be particularly useful in R&D and production environments where it is impossible to monitor the concentrations of intermediates in the reaction cycle and derive kinetic rate constants using methods similar to those used by Moscato et al. (2012, 2010) or the other mechanistic studies discussed earlier. Due to the inherent multistep nature of the reaction mechanism (seen in Scheme 2), the ability to predict rate constants from observable parameters may be useful for optimizing catalyst turnover, or producing polymer with consistent characteristics. The overall network fit results for this approach can be seen in Table 4, with the dataset passing the P and KS tests and having R²-value of 0.9755. Furthermore, the RMSE for the various kinetic parameters, as seen in Table 5, indicates that for all the parameters except the rate constant for Long Chain Branching (k_{lch}) , the errors are within a plausible margin. A surface plot of the prediction errors among different variables can be seen in Fig. 8. As with RMSE it is observed that for k_{lcb} (long chain branching) the error is larger than for the other

parameters, and the prediction has a stochastic nature to it. It is theorized that this constant is harder to predict because of the implicit nature of how a long chain branching event can only occur

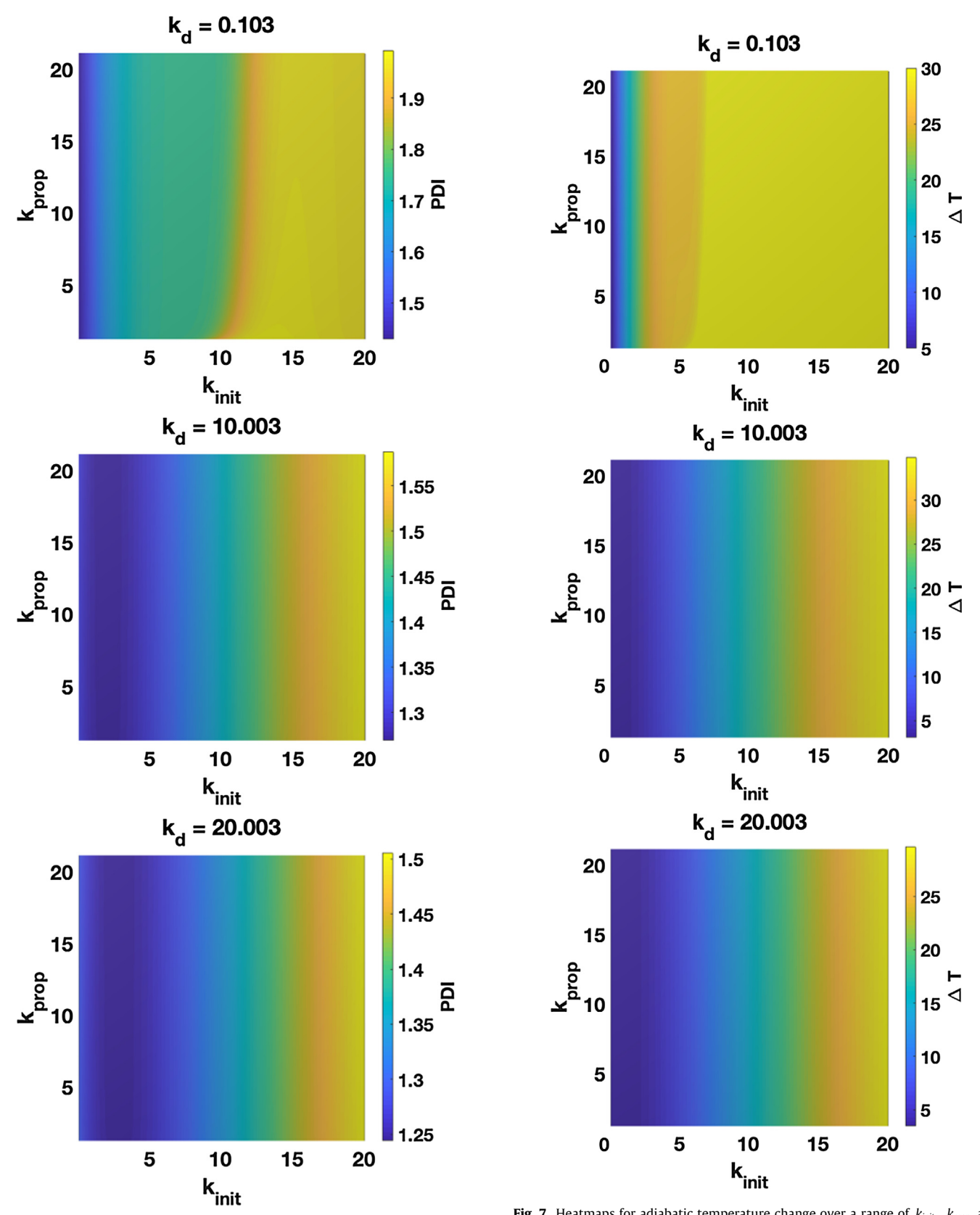


Fig. 6. Heatmaps for Θ over a range of k_{init} , k_{prop} and k_d .

Fig. 7. Heatmaps for adiabatic temperature change over a range of k_{init} , k_{prop} and k_d .

Table 4Statistical tests for reverse-trained network.

Statistical test	value
R^2	0.9755
P-test	0
KS-test	1

Table 5First parameters for reverse-trained network.

Data point	RMSE	RMSE (percent)
k _{init}	0.0627	-1.1780
k_{prop}	0.0004	0.3357
k_d	0.0365	-0.6604
k_{tM}	0.0749	-1.3561
k_{tCo}	0.1155	-1.9876
k_{eta}	0.0120	-0.4038
k_{lcb}	0.9954	-14.4118

when an activated polymer strand encounters a strand with a terminal double bond.

The reverse training method results in a slightly worse quality of fit over the forward network because three variables are being used to predict seven. This can be remedied by introducing more variables into the prediction algorithm, including the number of branched polymers, rate of polymerization, etc., but for the purposes of this study parameters were limited to those which could be easily measured in a laboratory environment. Overall though the reverse network plausibly predicts a possible combination of kinetic parameters.

4.4. Reaction rate constant prediction from incomplete data

The final step in this investigation was the use of a trained ANN for the prediction of kinetic rate constants from observable parameters which can be measured *ex situ*. Data was analyzed for catalysts used in previous publications in an attempt to derive kinetic rate constants from observable and recorded parameters and demonstrate the viability of the methodology. For this investigation a more basic neural network was trained, having weight

average molecular weight, number average molecular weight and D as inputs and the kinetic rate constants for initiation and propagation as outputs, essentially the reverse of the network constructed above. The reason for this smaller I/O network was due to the limitations of data available in previous publications, along with a trend in literature to report mainly just k_{init} and k_{prop} . Neural network training was updated using adaptive learning and data from entries one and three from Table 1, and data was simulated for values from one and five. This was necessary because the previous analysis assumed poly(propylene) production and the entries in Table 1 are for poly(hexene), demonstrating the adaptability of this approach. The reverse trained network was then used to predict theoretical rate constants given experimental outcomes based on the training dataset.

Upon training the new network and adapting it using the two known values, the rest of the experimental values from the literature were run through the analysis and results for the kinetic rate constants of initiation, propagation and termination were computed. The results for the predictions of the kinetic rate constants based on the weight average molecular weight can be seen in Fig. 9.

As a final step in the analysis a correlation matrix was computed between the three kinetic rate constants and the weight and number average molecular weights. The results from this calculation can be seen in Fig. 10 and show that there is a strong positive correlation between weight average molecular weight and the rate constant for initiation, and that the number average molecular weight is more impacted by the rate constant of propagation. Finally the analysis indicates, as expected, that the rate constant of termination negatively impacts both of the molecular weights.

5. Conclusions

From the forward network training results, it may be concluded that machine learning is a plausible method for approximating results for complex polymerization reactions based off of a first-principles training model using differential species balances. An ANN approach was used to successfully predict polymer characteristics including molecular weight a polydispersity in a forward direction from kinetic constants and in a reverse direction to predict kinetic constants from these observable parameters. This has

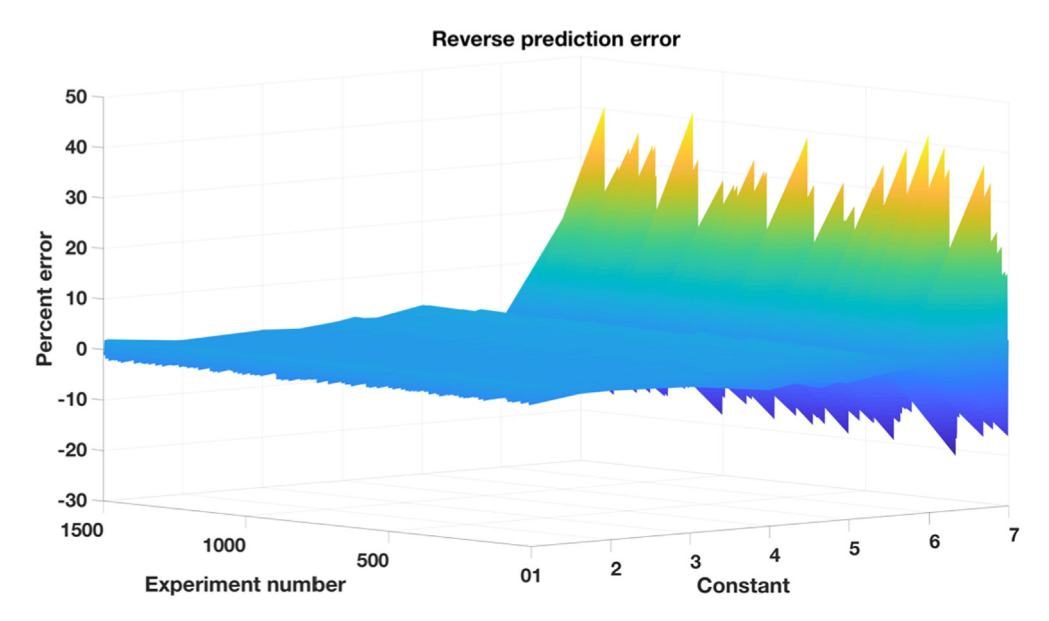


Fig. 8. Reverse prediction percent error for an ANN versus the constants (in order k_{init} , k_{prop} , k_d , k_{tM} , k_{tCo} , k_{β} , and k_{lcb}) and the experiment number. It is observed that k_{lcb} has the largest error.

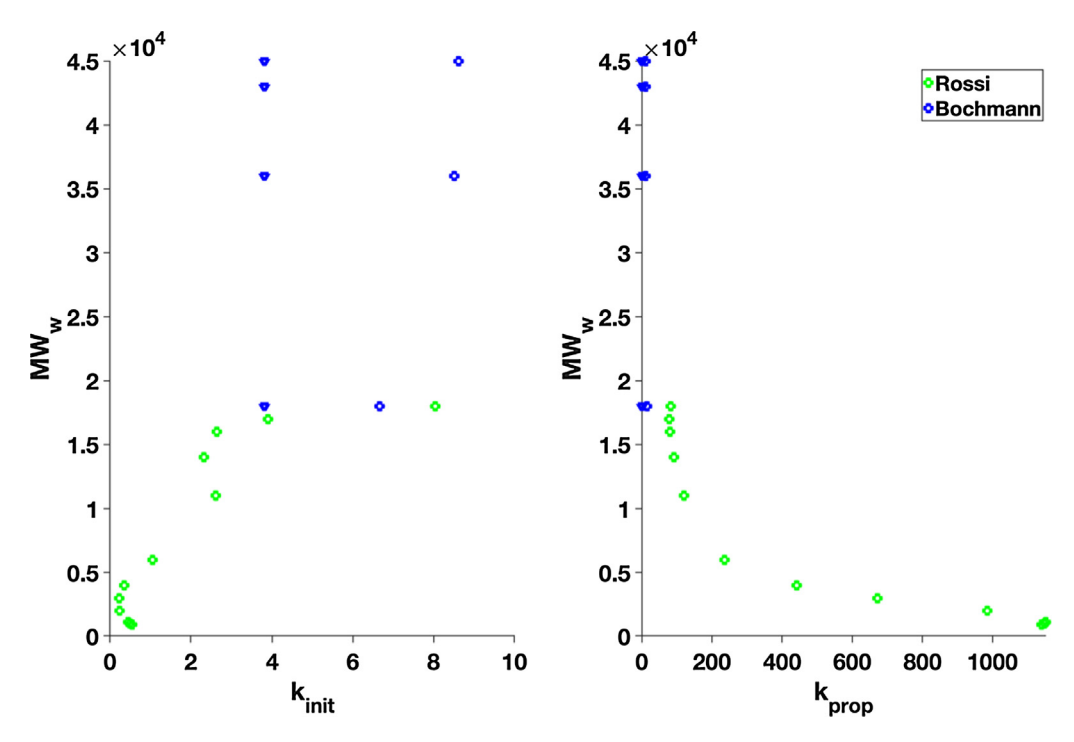


Fig. 9. Reverse prediction for the kinetic rate constants for propagation and initiation. Green circles represent predicted data from Zhao et al. (2000), blue circles represent predicted data from Ghiotto et al. (2013), with the triangles representing confirmation data. (For interpretation of the references to color in this figure legend, the reader is referred to the web version of this article.)

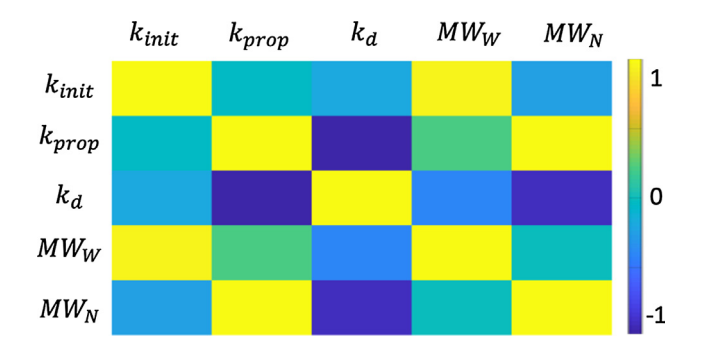


Fig. 10. Correlation coefficients between three key kinetic parameters and molecular weight information, with yellow hues representing a strong positive correlation and blue hues a negative one. (For interpretation of the references to color in this figure legend, the reader is referred to the web version of this article.)

implications both on the intelligent design of reactor systems and on the understanding of the process as a whole.

From analyzing the data produced by the forward training algorithm it is possible to make some conclusions about the catalyst. First, it is possible to see that there is a region of suboptimal operation at low rates of k_{init} , k_{prop} and k_d where the Θ is higher than in neighboring regions. This has implications for industrial reactors and production systems where the Θ is desired to be low. It is also noted that at low k_d the molecular weight increased. Additionally, it is observed that the number average molecular weight is related to the ratio between k_{prop} and k_d . Overall this demonstrated that ANNs can be used as a tool to try to ascertain complex behavior from kinetic systems.

Upon analyzing the data from the reverse training methodology certain conclusions can also be drawn about this catalyst system, including the possible rate constants of initiation, propagation and termination given information of the weight average and num-

ber average molecular weights. Additionally, information was provided on the strength of relationships between these variables, which indicated that a high rate constant of initiation negatively impacts the number average molecular weight for polymer chains. It should be noted that due to the lack of consistent and complete data in the literature, combined with secrecy in industrial R&D, these conclusions are drawn only upon a few publications, and further studies are necessary to enhance understanding in this field.

By training a neural network to 'understand' an experimental space for a particular catalyst, it was demonstrated that various properties of the resultant polymer could be predicted. By using data from these predictions, scientists could more quickly narrow down desired experimental spaces, and engineers could better understand scaleup considerations, among other uses. The reverse training allows for the prediction of kinetic constants from observable data, which has implications for robust process control. By being able to monitor properties of a system in-line it becomes possible to have a robust link between the reaction mechanism and reactor performance. This could allow for safer reactor operation by bringing machine learning as a tool to prevent situations where reaction runaway could occur. An additional use could be for the fine-tuning of large industrial reactors as minor changes in the reaction regime can strongly influence the properties of the final polymer, which has implications for the marketability and industrial applicability. It is generally considered that polymers with longer chains and lower PDIs have better mechanical properties, and it is desirable to ensure production in the regime which optimizes these characteristics. It is also beneficial to understand the degree of branching, both long chain and short chain, as these characteristics also influence the final composition and properties of the polymer. This could also have applications in the development of new polymers and processing techniques for 3D printer filaments and other specialized applications. Overall the AI-based link between reaction rate constants and observable parameters has implications in different areas of polymer science and engineering.

Funding sources

This material is based upon work supported by the National Science Foundation under Grant Number CBET-1701393. Any opinions, findings, and conclusions or recommendations expressed in this material are those of the authors and do not necessarily reflect the views of the National Science Foundation.

Declaration of Competing Interest

The authors declare that they have no known competing financial interests or personal relationships that could have appeared to influence the work reported in this paper.

Acknowledgements

The authors would like to thank Albert Shkolnik for his help in the literature search and Mark M. Green of the NYU Tandon School of Engineering for constantly making themselves available for questions and consultation throughout the publication process.

Appendix A. Supplementary material

Supplementary data to this article can be found online at https://doi.org/10.1016/j.ces.2019.115224.

References

- Ahmadi, M., Nekoomanesh, M., Arabi, H., 2009. New approach in modeling of metallocenecatalyzed olefin polymerization using artificial neural networks. Macromol. Theor. Simulat. 18, 195–200. https://doi.org/ 10.1002/mats.200800088.
- Bochmann, M., Lancaster, S.J., Hursthouse, M.B., Malik, K.M.A., 1994. Synthesis of base-free cationic zirconium methyl and benzyl complexes. the crystal and molecular structure of {C5H3(SiMe3), 2-1,3}2ZrMe(μ-Me)B(C6F5)3. Organometallics 13, 2235–2243. https://doi.org/10.1021/om00018a017.
- Chan, W.-M., Nascimento, C.A.O., 1994. Use of neural networks for modeling of olefin polymerization in high pressure tubular reactors. J. Appl. Polym. Sci. 53, 1277–1289. https://doi.org/10.1002/app.1994.070531002.
- Charoenpanich, T., Anantawaraskul, S., Soares, J.B.P., 2016. Estimation of polymerization conditions needed to make ethylene/1-olefin copolymers with specific microstructures using artificial neural networks. Macromol. React. Eng. 10, 215–232. https://doi.org/10.1002/mren.201500048.
- Chen, E.Y.X., Marks, T.J., 2000. Cocatalysts for metal-catalyzed olefin polymerization: activators, activation processes, and structure-activity relationships. Chem. Rev. 100, 1391–1434. https://doi.org/10.1021/cr980462j.
- Christianson, M.D., Tan, E.H.P., Landis, C.R., 2010. Stopped-flow NMR: determining the kinetics of [rac -(C2H 4(1-indenyl)2)ZrMe][MeB(C6F5) 3]-catalyzed polymerization of 1-hexene by direct observation. J. Am. Chem. Soc. 132, 11461–11463. https://doi.org/10.1021/ja105107y.
- Christopher, J.N., Diamond, G.M., Jordan, R.F., Petersen, J.L., 1996. Synthesis, structure, and reactivity of rac -Me ₂ Si(indenyl) ₂ Zr(NMe ₂) 2. Organometallics 15, 4038–4044. https://doi.org/10.1021/om960104b.
- Cruz, V., Ramos, J., Muñoz-Escalona, A., Lafuente, P., Peña, B., Martinez-Salazar, J., 2004. 3D-QSAR analysis of metallocene-based catalysts used in ethylene polymerisation. Polymer (Guildf). 45, 2061–2072. https://doi.org/10.1016/j. polymer.2003.12.059.
- Cruz, V.L., Martinez, J., Martinez-Salazar, J., Ramos, J., Reyes, M.L., Toro-Labbe, A., Gutierrez-Oliva, S., 2007a. QSAR model for ethylene polymerisation catalysed by supported bis(imino)pyridine iron complexes. Polymer (Guildf). 48, 7672–7678. https://doi.org/10.1016/j.polymer.2007.11.011.
- Cruz, V.L., Martinez, S., Martinez-Salazar, J., Polo-Cerón, D., Gómez-Ruiz, S., Fajardo, M., Prashar, S., 2007b. 3D-QSAR study of ansa-metallocene catalytic behavior in ethylene polymerization. Polymer (Guildf). 48, 4663–4674. https://doi.org/10.1016/j.polymer.2007.05.081.
- Cruz, V.L., Martinez, S., Ramos, J., Martinez-Salazar, J., 2014. 3D-QSAR as a tool for understanding and improving single-site polymerization catalysts. A review. Organometallics 33, 2944–2959. https://doi.org/10.1021/om400721v.
- Cruz, V.L., Ramos, J., Martinez, S., Muñoz-Escalona, A., Martinez-Salazar, J., 2005. Structure-activity relationship study of the metallocene catalyst activity in ethylene polymerization. Organometallics 24, 5095–5102. https://doi.org/ 10.1021/om050458f.
- Curteanu, S., Dragoi, E.-N., Leon, F., Butnariu, C., 2014. Artificial intelligence modelling methodologies applied to a polymerization process. In: Proc. 4th Int. Conf. Simul. Model. Methodol. Technol. Appl. pp. 43–49. https://doi.org/10. 5220/0005029800430049

- Curteanu, S., Leon, F., 2008. Optimization strategy based on genetic algorithms and neural networks applied to a polymerization process. Int. J. Quantum Chem. 108, 617–630. https://doi.org/10.1002/qua.21376.
- D'Agnillo, L., Soares, J.B.P., Penlidis, A., 1998. Effect of operating conditions on the molecular weight distribution of polyethylene synthesized by soluble metallocene/methylaluminoxane catalysts. Macromol. Chem. Phys. 199, 955–962. https://doi.org/10.1002/(SICI)1521-3935(19980601)199:6<955::AID-MACP955<3.0.CO;2-E.
- Dare, E.O., Ogunniyi, D.S., Olatunji, G.A., Chattopadhyay, P., 2004. Polymerization of propene with tBuNSiMe2C 5Me4TiMe2: effects of trialkylaluminiums as additives. Bull. Chem. Soc. Ethiop. 18, 131–141.
- Diwekar, U.M., Madhavan, K.P., 1991. Multicomponent batch distillation column design. Ind. Eng. Chem. Res. 30, 713–721. https://doi.org/10.1021/ie00052a014.
- Drummond, M.L., Sumpter, B.G., 2007. Use of drug discovery tools in rational organometallic catalyst design. Inorg. Chem. 46, 8613–8624. https://doi.org/10.1021/ic700670s.
- Ewen, J.A., 1984. Mechanisms of stereochemical control in propylene polymerizations with soluble group 4B metallocene/methylalumoxane catalysts. J. Am. Chem. Soc. 106, 6355-6364. https://doi.org/ 10.1021/ja00333a041.
- Fazilat, H., Akhlaghi, S., Shiri, M.E., Sharif, A., 2012. Predicting thermal degradation kinetics of nylon6/feather keratin blends using artificial intelligence techniques. Polymer (Guildf). 53, 2255–2264. https://doi.org/10.1016/j. polymer.2012.03.053.
- Galli, P., Cecchin, G., Chadwick, J.C., Del Duca, D., Vecellio, G., 2011. Polypropylene: 44 years young! The challenge for the 21st century. Met. Catal. Synth. Polym. 14–29. https://doi.org/10.1007/978-3-642-60178-1_2.
- Ghiotto, F., Pateraki, C., Severn, J.R., Friederichs, N., Bochmann, M., 2013. Rapid evaluation of catalysts and MAO activators by kinetics: what controls polymer molecular weight and activity in metallocene/MAO catalysts? Dalt. Trans. 42, 9040–9048. https://doi.org/10.1039/c3dt00107e.
- Giro, R., Cyrillo, M., Galvão, D.S., 2005. Using artificial intelligence methods to design new conducting polymers. Mater. Res. 6, 523–528. https://doi.org/ 10.1590/s1516-14392003000400017.
- Goncalves, V., Maria, K., da Silv, A.B.F., 2013. Applications of artificial neural networks in chemical problems. In: Artificial Neural Networks Architectures and Applications. InTech. https://doi.org/10.5772/51275.
- Gonzalez-Ruiz, R.A., Quevedo-Sanchez, B., Laurence, R.L., Henson, M.A., Bryan Coughlin, E., 2006. Kinetic modeling of slurry propylene polymerization using rac-Et(Ind) 2 ZrCl 2 /MAO. AIChE J. 52, 1824–1835. https://doi.org/10.1002/aic.10758.
- Guo, Y., Zhang, Z., Guo, W., Khan, A., Fu, Z., Xu, J., Fan, Z., 2017. Kinetics and mechanism of metallocene-catalyzed olefin polymerization: comparison of ethylene, propylene homopolymerizations, and their copolymerization. J. Polym. Sci. Part A Polym. Chem. 55, 867–875. https://doi.org/10.1002/ pola.28439.
- Herrmann, W.A., Rohrmann, J., Herdtweck, E., Spaleck, W., Winter, A., 1989. The first example of an ethylene-selective soluble ziegler catalyst of the zirconocene class. Angew. Chemie Int. Ed. English 28, 1511–1512. https://doi.org/10.1002/anie.198915111.
- Hildenbrand, P., Ahrens, W., Brandstetter, F., Simak, P., 1982. The formation of terminal double bonds in vinyl chloride polymerization. J. Macromol. Sci. Part A - Chem. 17, 1093–1106. https://doi.org/10.1080/00222338208066469.
- Himmelblau, D.M., 2000. Applications of artificial neural networks in chemical engineering. Korean J. Chem. Eng. 17, 373–392. https://doi.org/10.1007/BF02706848.
- Hölscher, M., Keul, H., Höcker, H., 2002. Explanation of the different reaction behaviors of bridged and unbridged cationic single component zirconocene catalysts in MMA polymerizations: a density functional study. Macromolecules 35, 8194–8202. https://doi.org/10.1021/ma020413f.
- Hough, B.R., Beck, D.A.C., Schwartz, D.T., Pfaendtner, J., 2017. Application of machine learning to pyrolysis reaction networks: reducing model solution time to enable process optimization. Comput. Chem. Eng. 104, 56–63. https://doi.org/10.1016/ j.compchemeng.2017.04.012.
- Hutley, T.J., Ouederni, M., 2016. Polyolefins—The history and economic impact, polyolefin compounds and materials. https://doi.org/10.1007/978-3-319-25982-6_2.
- lbrehem, A.S., Hussain, M.A., Ghasem, N.M., 2008. Mathematical model and advanced control for gas-phase olefin polymerization in fluidized-bed catalytic reactors. Chinese J. Chem. Eng. 16, 84–89. https://doi.org/10.1016/S1004-9541(08)60042-7.
- Inkson, N.J., Das, C., Read, D.J., 2006. Monte carlo simulation for the structure of polyolefins made with two metallocene catalysts in a batch reactor. Macromolecules 39, 4920–4931. https://doi.org/10.1021/ma060654d.
- Irfan, M.F., Mjalli, F.S., Kim, S.D., 2012. Modeling of NH 3-NO-SCR reaction over CuO/ γ -Al 2O 3 catalyst in a bubbling fluidized bed reactor using artificial intelligence techniques. Fuel 93, 245–251. https://doi.org/10.1016/j.fuel.2011.09.043.
- Kaminsky, W., 2011. Metalorganic Catalysts for Synthesis and Polymerization, Metalorganic Catalysts for Synthesis and Polymerization. Springer. https://doi. org/10.1007/978-3-642-60178-1.
- Kaminsky, W., 1994. Zirconocene catalysts for olefin polymerization. Catal. Today 20, 257–271. https://doi.org/10.1016/0920-5861(94)80005-7.
- Kaminsky, W., Külper, K., Brintzinger, H.H., Wild, F.R.W.P., 1985. Polymerization of propene and butene with a chiral zirconocene and methylalumoxane as cocatalyst. Angew. Chemie Int. Ed. English 24, 507–508. https://doi.org/ 10.1002/anie.198505071.

- Kaminsky, W., Spiehl, R., 1989. Copolymerization of cycloalkenes with ethylene in presence of chiral zirconocene catalysts. Die Makromol. Chemie 190, 515–526. https://doi.org/10.1002/macp.1989.021900308.
- Kaminsky, W., Steiger, R., 1988. Polymerization of olefins with homogeneous zirconocene/alumoxane catalysts. Polyhedron 7, 2375–2381. https://doi.org/ 10.1016/S0277-5387(00)86355-X.
- Kawamura-Kuribayashi, H., Koga, N., Morokuma, K., 1992. An ab Initio MO and MM study of homogeneous olefin polymerization with silylene-bridged zirconocene catalyst and its regio- and stereoselectivity. J. Am. Chem. Soc. 114, 8687–8694. https://doi.org/10.1021/ja00048a049.
- Kim, I., Nam Hwang, G., 1998. Isospecific polymerization of propylene by ansa zirconocene diamide compound cocatalyzed by Mao. J. Macromol. Sci. Part A 35, 1987–2008. https://doi.org/10.1080/10601329808000992.
- Kite, S., Hattori, T., Murakami, Y., 1994. Estimation of catalytic performance by neural network - product distribution in oxidative dehydrogenation of ethylbenzene. Appl. Catal. A, Gen. 114, L173–L178. https://doi.org/10.1016/ 0926-860X(94)80169-X.
- Kolthammer, B.W.S., Mangold, D.J., Gifford, D.R., 1992. Polymerization kinetics of octene-1 catalyzed by metallocene methylaluminoxane investigated with attenuated total reflectance fourier transform infrared (ATR-FT-IR) spectroscopy. J. Polym. Sci. Part A Polym. Chem. 30, 1017–1026. https://doi. org/10.1002/pola.1992.080300607.
- Krauledat, H., Brintzinger, H.-H., 1990. Isotope effects associated with α-olefin insertion in zirconocene-based polymerisation catalysts: evidence for an αagostic transition state. Angew. Chemie Int. Ed. English 29, 1412–1413. https:// doi.org/10.1002/anie.199014121.
- Leite, M.S., Ferreira, B., Maria, L., Lona, F., Silva, V., Maria, A., Fileti, F., 2007. Application of Artificial Intelligence Techniques for Temperature Prediction in a Polymerization Process. Univ. Campinas.
- Lenton, T.N., Bercaw, J.E., Panchenko, V.N., Zakharov, V.A., Babushkin, D.E., Soshnikov, I.E., Talsi, E.P., Brintzinger, H.H., 2013. Formation of trivalent zirconocene complexes from ansa-zirconocene-based olefin-polymerization precatalysts: an EPR- and NMR-spectroscopic study. J. Am. Chem. Soc. 135, 10710–10719. https://doi.org/10.1021/ja403170u.
- Lin, S., Tagge, C.D., Waymouth, R.M., Nele, M., Collins, S., Pinto, J.C., 2000. Kinetics of propylene polymerization using bis(2-phenylindenyl)zirconium dichloride/ methylaluminoxane. J. Am. Chem. Soc. 122, 11275–11285. https://doi.org/ 10.1021/ja002003h.
- Liu, Z., Somsook, E., White, C.B., Rosaaen, K.A., Landis, C.R., 2001. Kinetics of initiation, propagation, and termination for the [rac-(C2H4(1-indenyl)2)ZrMe] [MeB(C 6F5)3]-catalyzed polymerization of 1-hexene. J. Am. Chem. Soc. 123, 11193-11207. https://doi.org/10.1021/ja016072n.
- MacGregor, J.F., 1986. Control of polymerization reactors. IFAC Proc. 19, 31–35. https://doi.org/10.1016/S1474-6670(17)59395-7.
- Martínez, S., Cruz, V.L., Ramos, J., Martínez-Salazar, J., 2012. Polymerization activity prediction of zirconocene single-site catalysts using 3D quantitative structureactivity relationship modeling. Organometallics 31, 1673–1679. https://doi.org/ 10.1021/om2007776.
- Mohd Ali, J., Hussain, M.A., Tade, M.O., Zhang, J., 2015. Artificial Intelligence techniques applied as estimator in chemical process systems - A literature survey. Expert Syst. Appl. 42, 5915–5931. https://doi.org/10.1016/j. eswa.2015.03.023.
- Möhring, P.C., Coville, N.J., 2006. Group 4 metallocene polymerisation catalysts: quantification of ring substituent steric effects. Coord. Chem. Rev. 250, 18–35. https://doi.org/10.1016/j.ccr.2005.01.024.
- Molga, E.J., Van Woezik, B.A.A., Westerterp, K.R., 2000. Neural networks for modelling of chemical reaction systems with complex kinetics: oxidation of 2-octanol with nitric acid. Chem. Eng. Process. Process Intensif. 39, 323–334. https://doi.org/10.1016/S0255-2701(99)00093-8.
- Moscato, B.M., Zhu, B., Landis, C.R., 2012. Mechanistic investigations into the behavior of a labeled zirconocene polymerization catalyst. Organometallics 31, 2097–2107. https://doi.org/10.1021/om3000955.
 Moscato, B.M., Zhu, B., Landis, C.R., 2010. GPC and ESI-MS analysis of labeled poly(1-
- Moscato, B.M., Zhu, B., Landis, C.R., 2010. GPC and ESI-MS analysis of labeled poly(1-hexene): rapid determination of initiated site counts during catalytic alkene polymerization reactions. J. Am. Chem. Soc. 132, 14352–14354. https://doi.org/10.1021/ja105775r.
- Nakazaki, Y., Inui, T., 1989. Highly selective decomposition of methanol to syngas on nickel-based composite catalysts using an artificial intelligence control reactor system. Ind. Eng. Chem. Res. 28, 1285–1289. https://doi.org/10.1021/ie00093a003.
- Nandi, S., Mukherjee, P., Tambe, S.S., Kumar, R., Kulkarni, B.D., 2002. Reaction modeling and optimization using neural networks and genetic algorithms: case study involving TS-1-catalyzed hydroxylation of benzene. Ind. Eng. Chem. Res. 41, 2159–2169. https://doi.org/10.1021/ie010414g.
- Nayak, A., Gupta, S.K., 2004. Multi-objective optimization of semi-batch copolymerization reactors using adaptations of genetic algorithm. Macromol. Theory Simulations 13, 73–85. https://doi.org/10.1002/mats.200350033.
- Paass, G., 1993. Assessing and improving neural network predictions by the bootstrap algorithm. Adv. Neural Inf. Process. Syst. 5, 196–203.
- Papes Filho, A.C., Maciel Filho, R., 2010. Hybrid training approach for artificial neural networks using genetic algorithms for rate of reaction estimation: application to industrial methanol oxidation to formaldehyde on silver catalyst. Chem. Eng. J. 157, 501–508. https://doi.org/10.1016/j.cej.2009.12.045.

- Pletcher, P.D., Switzer, J.M., Steelman, D.K., Medvedev, G.A., Delgass, W.N., Caruthers, J.M., Abu-Omar, M.M., 2016. Quantitative comparative kinetics of 1-hexene polymerization across group IV bis-phenolate catalysts. ACS Catal. 6, 5138-5145. https://doi.org/10.1021/acscatal.6b00974.
- Polikar, R., Shinar, R., Udpa, L., Porter, M.D., 2001. Artificial intelligence methods for selection of an optimized sensor array for identification of volatile organic compounds. Sens. Actuat., B Chem. 80, 243–254. https://doi.org/10.1016/ S0925-4005(01)00903-0.
- Prakash, N., 2013. Kinetic Modeling and Simulation of Metallocene Catalyzed Olefin Polymerization. Birla Institute of Technology and Science (BITS).
- Resconi, L., 1999. Chain transfer and isomerization reactions in propylene polymerization with isospecific metallocene catalysts. Polym. Mater. Sci. Eng. Div. 80, 421. https://doi.org/10.1023/A:1019115801193.
- Rieger, B., Janiak, C., 1994. Concentration effects of methylalumoxane, zirconocene dichloride and trimethylaluminum in ethylene polymerization. Die Angew. Makromol. Chemie 215, 35–46. https://doi.org/10.1002/apmc.1994.052150104.
- Ruiz, D., Nougués, J.M., Calderón, Z., Espuña, A., Puigjaner, L., 2000. Neural network based framework for fault diagnosis in batch chemical plants. Comput. Chem. Eng. 24, 777–784. https://doi.org/10.1016/S0098-1354(00)00371-9.
- Sadiku, M.N.O., Musa, S.M., Musa, O.M., 2017. Machine learning in chemical industry. Int. J. Adv. Sci. Res. Eng. 4, 4618–4620. https://doi.org/10.7324/ ijasre.2017.32524.
- Sasaki, M., Hamada, H., Kintaichi, Y., Ito, T., 1995. Application of a neural network to the analysis of catalytic reactions analysis of NO decomposition over Cu/ZSM-5 zeolite. Appl. Catal. A, Gen. 132, 261–270. https://doi.org/10.1016/0926-860X (95)00171-9.
- Schwaller, P., Gaudin, T., Lányi, D., Bekas, C., Laino, T., 2018. "Found in Translation": predicting outcomes of complex organic chemistry reactions using neural sequence-to-sequence models. Chem. Sci. 9, 6091–6098. https://doi.org/10.1039/c8sc02339e.
- Soga, K., Kaminaka, M., 1993. Polymerization of propene with zirconocene-containing supported catalysts activated by common trialkylaluminiums. Die Makromol. Chemie 194, 1745–1755. https://doi.org/10.1002/macp.1993.021940621.
- Song, F., Cannon, R.D., Bochmann, M., 2004a. The kinetics of propene and hexene polymerisation with [(SBI)ZrR]+X-: evidence for monomer-dependent early or late transition states. Chem. Commun. 4, 542–543. https://doi.org/10.1039/b314845a.
- Song, F., Cannon, R.D., Bochmann, M., 2003. Zirconocene-catalyzed propene polymerization: a quenched-flow kinetic study. J. Am. Chem. Soc. 125, 7641– 7653. https://doi.org/10.1021/ja029150v.
- Song, F., Hannant, M.D., Cannon, R.D., Bochmann, M., 2004b. Zirconocene-catalysed propene polymerisation: kinetics, mechanism, and the role of the anion. Macromol. Symp. 213, 173–185. https://doi.org/10.1002/masy.200450917.
- Subramanyam, U., Sivaram, S., 2007. Kinetics of hexene-1 polymerization using [(N, N'-diisopropylbenzene)- 2,3-(1,8-napthyl)-1,4-diazabutadiene] dibromonickel/methylaluminoxane catalyst system. J. Polym. Sci. Part A Polym. Chem. 45, 1093–1100. https://doi.org/10.1002/pola.21852.
- Switzer, J.M., Travia, N.E., Steelman, D.K., Medvedev, G.A., Thomson, K.T., Delgass, W.N., Abu-Omar, M.M., Caruthers, J.M., 2012. Kinetic modeling of 1-hexene polymerization catalyzed by Zr(t Bu-ON NMe2O)Bn 2/B(C 6F 5) 3. Macromolecules 45, 4978–4988. https://doi.org/10.1021/ma300129n.
- Valeh-E-Sheyda, P., Yaripour, F., Moradi, G., Saber, M., 2010. Application of artificial neural networks for estimation of the reaction rate in methanol dehydration. Ind. Eng. Chem. Res. 49, 4620–4626. https://doi.org/10.1021/ie9020705.
- Wang, B., Mu, B., Deng, X., Cui, H., Xu, S., Zhou, X., Zou, F., Li, Yang, Yang, L., Li, Yufei, Hu, Y., 2005. Synthesis and structures of cycloalkylidene-bridged cyclopentadienyl metallocene catalysts: effects of the bridges of ansametallocene complexes on the catalytic activity for ethylene polymerization. Chem. A Eur. J. 11, 669–679. https://doi.org/10.1002/chem.200400750. Woo, H.G., Tilley, T.D., 1989. Dehydrogenative polymerization of silanes to
- Woo, H.G., Tilley, T.D., 1989. Dehydrogenative polymerization of silanes to polysilanes by zirconocene and hafnocene catalysts. A new polymerization mechanism. J. Am. Chem. Soc. 111, 8043–8044. https://doi.org/ 10.1021/ja00202a070.
- Yasin, T., Fan, Z., Feng, L., 2005. Effect of temperature on the isospecific propylene polymerization catalyzed by rac-dimethylsilylbis(2,4,6-trimethyl-1-indenyl) zirconium dichloride/methyl aluminoxane. Polyhedron 24, 1262–1268. https://doi.org/10.1016/j.poly.2005.02.013.
- Young, M.J., Ma, C.C.M., 2002. Polymerization kinetics and modeling of slurry ethylene polymerization process with metallocene/MAO catalysts. Polym. Plast. Technol. Eng. 41, 601–618. https://doi.org/10.1081/PPT-120006436.
- Yu, Y., Cipullo, R., Boisson, C., 2019. Alkynyl ether labeling: a selective and efficient approach to count active sites of olefin polymerization catalysts. ACS Catal. 9, 3098–3103. https://doi.org/10.1021/acscatal.8b04624.
- Zhang, Z., Friedrich, K., 2003. Artificial neural networks applied to polymer composites: a review. Compos. Sci. Technol. 63, 2029–2044. https://doi.org/10.1016/S0266-3538(03)00106-4.
- Zhao, X., Odian, G., Rossi, A., 2000. Kinetics, polymer molecular weights, and microstructure in zirconocene-catalyzed 1-hexene polymerization. J. Polym. Sci. Part A Polym. Chem. 38, 3802–3811. https://doi.org/10.1002/1099-0518 (20001015)38:20<3802::AID-POLA110>3.0.CO;2-N.